Chin. Sci. Bull. (2014) 59(33):4367–4378
DOI 10.1007/s11434-014-0567-0

csb.scichina.com
www.springer.com/scp

Article

Engineering Thermophysics

Development and dynamic characteristics of an Organic Rankine Cycle

Zheng Miao · Xufei Yang · Jinliang Xu · Jinghuang Zou

Received: 28 May 2014 / Accepted: 30 June 2014 / Published online: 9 August 2014

Abstract The design, construction and test of an Organic Rankine Cycle (ORC) with R123 as the working fluid were performed. A scroll expander was integrated in the system. The conductive oil with its temperature of 150 °C was used to simulate the low-grade heat source. An AC dynamometer unit measured the expander shaft torque, rotating speed and shaft power. The experiments were conducted in two operating modes: the constant mass flow rate and the constant shaft torque. Under the constant mass flow rate operating mode, the stepped increase of the shaft torque increased the expansion ratios of the expander and decreased the vapor superheats at the expander inlet. Thus, the shaft power and thermal efficiency were increased. Alternatively, the constant shaft torque operating mode involved two different regions, interfaced at the pumping frequency of 9 Hz. By the increase of the mass flow rates, the vapor superheats at the expander inlet was decreased and the shaft power was increased, but the ORC thermal efficiencies were slightly decreased. Both operating modes yielded the saturation shaft powers that were the maximum values one could use. It was found that the measured shaft powers and ORC thermal efficiencies were lower than the enthalpy determined values based on the fluid pressures and temperatures at the expander inlet and outlet. The maximum measured shaft power and thermal efficiency were 2.63 kW and 5.31 %, compared with the enthalpy determined values of 3.87 kW and 9.46 %, respectively.

SPECIAL TOPIC: Deep Utilization of Boiler Low-Temperature Flue Gas

Z. Miao · X. Yang · J. Xu (✉) · J. Zou
Beijing Key Laboratory of Multiphase Flow and Heat Transfer for Low Grade Energy Utilization, North China Electric Power University, Beijing 102206, China
e-mail: xjl@ncepu.edu.cn

Keywords Organic Rankine Cycle · Scroll expander · Shaft torque · Shaft power · Thermal efficiency

1 Introduction

The rapid increase in energy consumption all over the world has led to the demand for waste heat recovery from industries to increase the utilization efficiency of fossil energy sources. Besides, applications of the alternative energies such as geothermal heat, concentrating solar thermal energy and biomass energy should be further explored. Most of the waste heat and alternative energy belongs to the low-grade energy (temperature below 250 °C), accounting for more than 50 % of the total heat generation in the world [1]. The Organic Rankine Cycle (ORC) is one of the promising technologies to convert low-grade heat into work [2, 3]. Due to the low boiling point of organic fluids, the ORC system generates a higher vapor pressure for power generation, which is difficult to be fulfilled with a conventional water-steam Rankine system [4]. Thus, ORC has been extensively investigated theoretically and experimentally.

The first and second laws of the thermodynamics were often used to analyze the ORC performance. The literature survey showed the strong effect of the heat source temperatures on the selection of working fluids [5–9]. Liu et al. [5] analyzed the ORC performance influenced by working fluids. The wet fluids were not preferable for ORCs. The thermal efficiencies for various working fluids were a weak function of the critical temperatures. R123 was recommended by several groups [10–12], especially at the heat source temperature of about 400 K.

The ORC measurement is necessary before its commercial operation. R123, R245fa and other organic fluids were used in previous ORC prototypes. Yamamoto et al. [13] designed and tested an ORC, which showed a better performance of R123. Mathias et al. [14] tested a scroll expander and a gerotor in an ORC to generate power. The two expanders produced 2.07 and 2.96 kW work, having the isentropic efficiency of 85 % and 83 %, respectively. They claimed that both types of expanders were good candidates for ORCs. Lemort et al. [15–17] integrated an open-drive oil-free scroll expander in an ORC with R123 as the working fluid. The maximum overall isentropic effectiveness achieved 68 %. The heat loss, internal leakage and mechanical-induced exergy destructions mainly accounted for the weakened expander performance. Li et al. [18–20] investigated a kW-scale ORC using R123 as the working fluid. The specially designed and manufactured turbine had a rotating speed up to 60,000 r/min. They obtained the maximum turbine power of 1 kW, the isentropic efficiency of 0.65 and the thermal efficiency of 6.8 %, at the temperature drop of 70 K between the turbine inlet and condenser outlet. Bracco et al. [21] demonstrated and tested a domestic-scale ORC prototype (R245fa was the working fluid). A hermetic scroll expander was used. A global electric efficiency of about 8 % was obtained at the expander inlet temperature in the range of 120–150 °C. Li et al. [22] investigated the influence of mass flow rates on the regenerative ORC efficiencies. A single-stage axial flow turbine was adopted. The 6 kW power output and the regenerative ORC efficiency of 7.98 % were achieved at a heat source temperature of 130 °C.

In addition to the independent use of ORCs, ORCs were integrated with other energy systems. For instance, Manolakos et al. [23–25] experimentally evaluated a low-temperature solar heat-driven ORC coupled with a reverse osmosis (RO) desalination system. It was found that the solar radiation played a dominant role on the coupled system performance. The average ORC efficiencies were 0.73 % and 1.17 % for the cloudy and sunny days, respectively. Wang et al. [26–30] experimentally investigated a low-temperature solar recuperative ORC system using R245fa and some zeotropic mixtures as the working fluids. The overall efficiency of 2.42 % was obtained. They also dynamically tested the performance of a kW-scale rolling-piston expander. A maximum shaft power of 0.35 kW, steady isentropic efficiency of 40 % and thermal efficiency of 5 %–6 % were reported.

From the above literature review, it is seen that even though several experimental investigations have been performed, the small-scale ORC is still in the infancy stage. The ORC performance parameters (i.e., output work and thermal efficiency) were mainly calculated based on the enthalpy differences across the pump or expander. The enthalpy was decided by the fluid pressures and temperatures at the expander inlet and outlet as it is very hard to measure the fluid pressures and temperatures in the expansion chamber. Due to the pressure drop during the suction, heat loss from the expander to the air, over-expansion or under-expansion losses as well as the power losses using belts and couplings, the calculated shaft power and system thermal efficiency deviated from the practical values that one could use [15]. The directly measured shaft power of the expander and thermal efficiency of the ORC are seldom reported in the literature [15–17].

In this paper, an ORC system of 4 kW-scale power output capacity was built and tested. A scroll expander converted the heat into work. An AC dynamometer controlled the expander and measured the expander parameters. The ORC system was operating either in a constant mass flow rate operating mode or in a constant shaft torque operating mode. The dynamic response of the two operating modes was thoroughly discussed and analyzed. The measured shaft power and the ORC thermal efficiency were compared with the enthalpy determined values. It was found that the enthalpy determined shaft power of the expander and thermal efficiency of the ORC system were greatly overestimated. The heat source temperature entering the ORC evaporator was about 150 °C.

2 The ORC experimental setup

2.1 The ORC system design

The ORC system operates according to the Rankine cycle principle. The ideal cycle consisted of two isobaric heat transfer processes and two isentropic processes. The organic fluid was pumped into the evaporator at a high pressure to extract heat from the heat source. Then, the saturated or superheated vapor of the organic fluid expanded in the expander to generate work. The vapor or two-phase mixture leaving the expander was condensed to liquid in a condenser. The liquid was circulated by a pump. A practical ORC system was much complicated than an ideal cycle. Exergy destructions occurred in the pump and expander. The leakage of the organic fluid should be avoided. The heat transfer performance was poor for the organic fluid. Figure 1 shows the ORC flow loops in this study. The system consisted of five coupled subsystems: conductive oil circuit, R123 circuit, cooling water circuit, lubricant oil circuit and AC dynamometer unit. Figure 2 shows the ORC experimental setup, covering a planar size of about 3 m × 5 m.

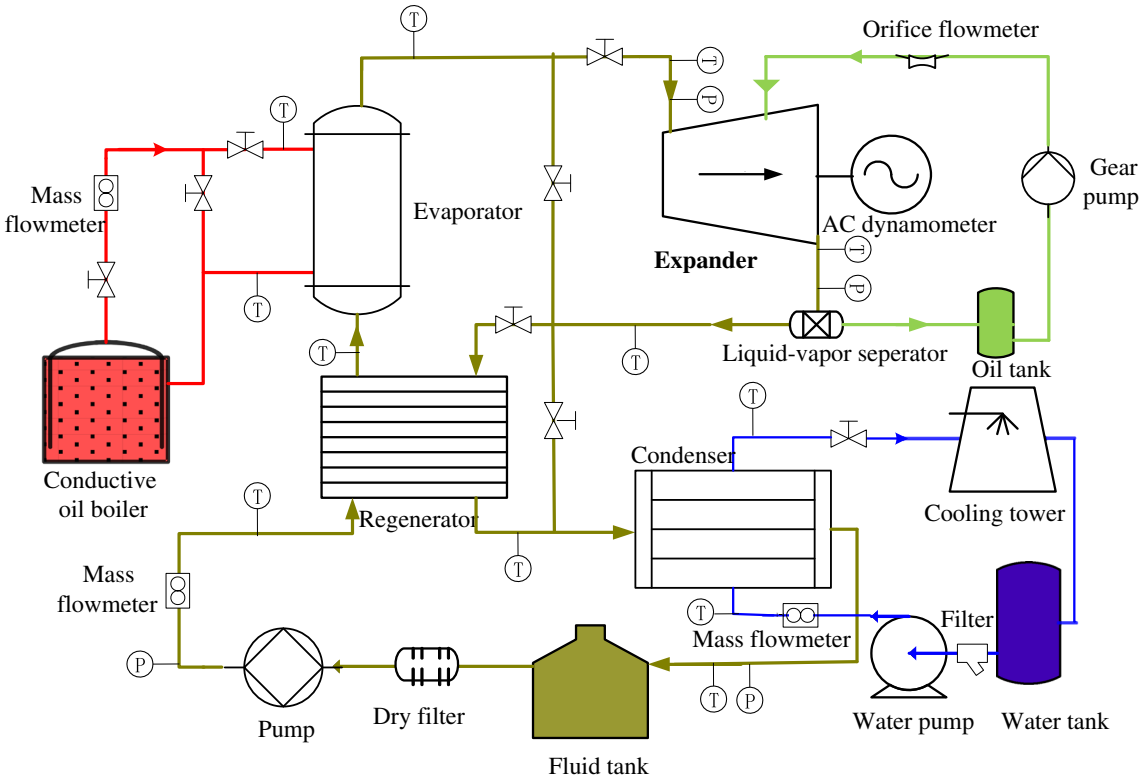

Fig. 1 (Color online) The schematic representation of the ORC system

2.1.1 *The conductive oil circuit*

The conductive oil was used as the heat carrier fluid of the low-grade heat source and was heated by an electric heater with the capacity of 100 kW. The oil temperature entering the ORC evaporator was manually set. The electric heater automatically adjusted the heating power to satisfy the required oil temperature. The maximum oil temperature could reach 250 °C. The temperature could be controlled with an uncertainty of 1 °C. An axial pump circulated the conductive oil, receiving the heat from the electric heater and dissipating the heat to the ORC evaporator.

2.1.2 *The R123 loop*

Based on the literature review above and the thermodynamic calculation in advance, R123 was chosen as the working fluid. The ORC loop consisted of a piston pump, an evaporator, an expander and a condenser. The regenerative heat exchanger was not used in this study. The R123 mass flow rate provided by the piston pump was controlled by a frequency converter (50 Hz frequency corresponding to volume flow rate of about 2,000 L/h). The evaporator was a tube-in-tube heat exchanger, having a heat transfer area of 5.53 m^2. The condenser was a plate heat exchanger, having a heat transfer area of 6.08 m^2.

The expander was modified from a scroll compressor for the bus-used air-conditioning system. Because the compressor has simple structure and high reliability and it is available commercially, it is considered as one of the promising candidates for the expander in kW-scale capacity. Figure 2b shows the fixed and rotating scrolls. Table 1 gives the detailed geometrical parameters. Some modifications were performed so that it was suitable to work as an expander. The maximum shaft power of the expander was about 4 kW.

The pressure and temperature sensors were arranged at various locations of the ORC system (see Fig. 1). The heating power received by the evaporator was

$$Q = m(h_{\mathrm{eva,out}} - h_{\mathrm{eva,in}}), \tag{1}$$

where m is R123 the mass flow rate, $h_{\mathrm{eva,out}}$ and $h_{\mathrm{eva,in}}$ are the R123 enthalpies at the evaporator outlet and inlet, respectively. The two enthalpies were determined by the pressures and temperatures at the evaporator outlet and inlet, respectively. The fluid was subcooled liquid at the evaporator inlet and superheated vapor at the evaporator outlet. The two-phase mixture state at the evaporator outlet was not encountered.

During the expansion process, the calculated shaft power of the expander was

$$W_{\mathrm{t,cal}} = m(h_{\mathrm{t,in}} - h_{\mathrm{t,out}}), \tag{2}$$

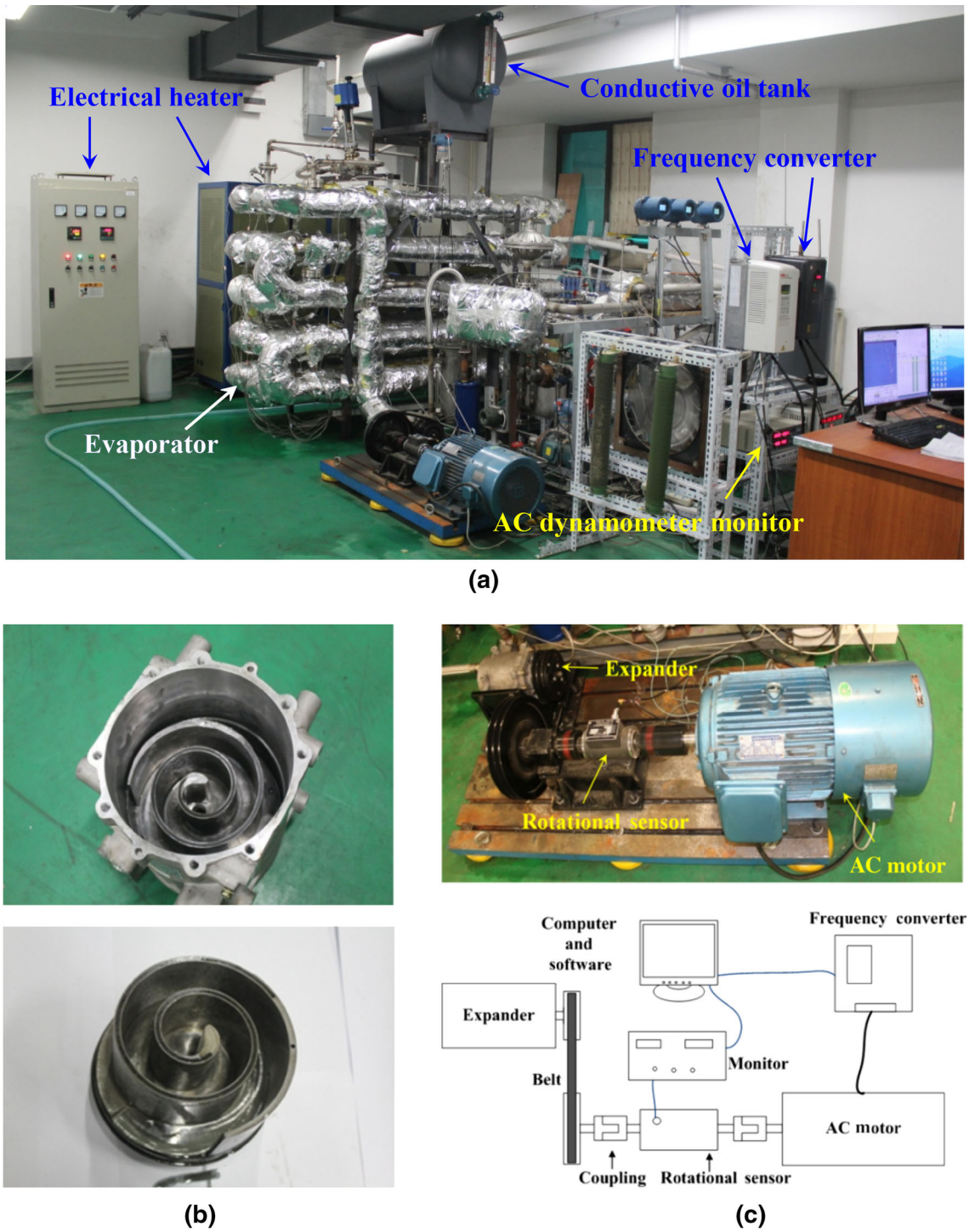

Fig. 2 (Color online) The photo of the experimental setup (**a**), the fixed and rotating scrolls of the expander (**b**) and the AC dynamometer unit (**c**)

where $h_{t,in}$ and $h_{t,out}$ are the enthalpies at the expander inlet and outlet. The real expansion process is an entropy-increase process and the isentropic efficiency was

$$\eta_{t,s} = \frac{h_{t,in} - h_{t,out}}{h_{t,in} - h_{t,s,out}}, \tag{3}$$

where $h_{t,s,out}$ was the enthalpy at the expander outlet for the isentropic expansion process, which could be deduced from the expander inlet entropy and expander outlet pressure.

The pumping power was

$$W_{p,cal} = m(h_{p,out} - h_{p,in}), \tag{4}$$

Table 1 The structure parameters of the scroll expander

Parameters	Value
Scroll turns	2.5
Height of the scroll profile	50 mm
Thickness of the scroll profile	4.8 mm
Pitch of the scroll profile	26.5 mm
Radius of the expander	170 mm
Length of the expander	281 mm

where $h_{p,out}$ and $h_{p,in}$ are the fluid enthalpies at the pump outlet and inlet, respectively. Thus, the calculated "net" output work of the ORC system was

$$W_{cal} = W_{t,cal} - W_{p,cal}. \quad (5)$$

The calculated thermal efficiency of the ORC system was

$$\eta_{cal} = \frac{W_{cal}}{Q} = \frac{W_{t,cal} - W_{p,cal}}{Q}. \quad (6)$$

The calculated thermal efficiency, η_{cal}, was based on the measured pressures and temperatures at various locations. Attention should be paid to the shaft power of the expander. As mentioned above, due to the difficulties in directly measuring temperature and pressure at the expansion chamber, sensors are located at the expander inlet and outlet. Thus, the calculated enthalpy drop across the expander cannot be fully converted into the shaft power. Part of it was consumed by the pressure drop during the suction, heat loss from the expander to the air, over-expansion or under-expansion losses as well as the power losses using belts and couplings. Besides, the exergy destruction existed in the piston pump. The pumping power should be larger than that decided by the enthalpy rise across the pump. Therefore, the calculated thermal efficiency overestimated the real value. In this study, an AC dynamometer unit measured the rotating speed, shaft torque and shaft power for the expander (see later subsections). The real pumping power was measured by a pump frequency converter.

2.1.3 The cooling water loop

The cooling water loop was thermally coupled with the ORC condenser. It dissipated the extra heat of the ORC system to the air environment. The outdoor spray cooling tower was the key component of the cooling water loop. The tower had the cooling capacity of about 73 kW, corresponding to the water flow rate of 5,000 kg/h, at which the temperature difference of the cooling water loop was 5 °C.

2.1.4 The lubricant oil loop

The expander operating needed lubricant. A gear pump circulated the lubricant. The lubricant was mixed with the R123 vapor at the expander inlet. After the expansion, the lubricant was separated from the R123 vapor by an efficient vapor-oil separator. Then, the lubricant returned to the oil tank.

2.1.5 The AC dynamometer unit

Figure 2c shows the AC dynamometer, dynamically measuring the rotating speed, shaft torque and shaft power of the expander. The unit consisted of a frequency converter, an AC motor, a rotating speed sensor, a monitor, a software and transmission facilities. The shaft power was transmitted by a belt and couplings to the AC motor. The rated rotating speed and the maximum shaft torque of the AC motor were 1,480 r/min and 78.5 N m, respectively. The rotating speed of the expander was two times of that of the AC motor. The computer software dynamically processed the rotating speed and the shaft torque of the expander with the help of sensors. The software communicated with the frequency converter to control the shaft torque of the AC motor. During the system operating, the shaft torque of the AC motor was set by the software to be a specific percentage of the maximum value (78.5 N m here). The frequency converter of the AC motor controlled the shaft torque to maintain the desired value. In such a way, the shaft power of the expander and the pumping power were directly measured. The measured shaft power and the thermal efficiency were

$$W_{me} = W_{t,me} - W_{p,me}, \quad (7)$$

$$\eta_{me} = \frac{W_{t,me} - W_{p,me}}{Q}, \quad (8)$$

where the subscript of "me" stands for the measured value. The net power, W_{me}, is the expander shaft power subtracting the pumping power.

2.2 The operating procedure

The fluid state parameters were the pressures and temperatures at the inlet and outlet of various components (see Fig. 1). The mass flow rates were measured for the conductive oil, R123 fluid and cooling water. The rotating speed, shaft torque, shaft power of the expander and the piston pump consumed power were measured by the hardware mentioned in Sect. 2.1. Table 2 shows the uncertainties of various measurements.

From the thermodynamic point of view, the ORC system could be operating by specifying the mass flow rate, pressures and temperatures of the organic fluid. For this ORC prototype, the closed ORC system was initially vacuumed to remove the non-condensable gas. Then, the system was charged by a certain limit of R123 liquid. In

such a way, part of the ORC internal volume was occupied by the R123 liquid, and part of the volume was occupied by the R123 vapor. The R123 pressures and temperatures at various locations were not independent parameters during the system operating, but they were determined by the mass flow rate of the R123 fluid and the external load of the expander such as the shaft torque and shaft power. This study involved two operating modes: the constant mass flow rate operating mode and the constant shaft torque operating mode.

Table 3 shows the major operating parameters. The conductive oil had a constant mass flow rate and temperature before entering the ORC evaporator. The cooling water temperature entering the condenser varied in a narrow range for changed environment temperatures and the condenser load. At the piston pump frequency of 10 Hz, the shaft torque of the expander was changed from 10 % to 50 % of the maximum torque load. Alternatively, at the shaft torque of 40 % of the maximum torque load, the R123 piston pump frequency was changed from 5 to 11 Hz.

Table 2 The parameter measurements and uncertainties

Parameters	Sensors	Range	Accuracy
Temperature	K-type thermocouple	−200–1,300 °C	±0.5 °C
Pressure	Rosemount 3051 CG	0–1 MPa 0–5 MPa	±0.1 % F.S
Pressure difference	Rosemount 3051 CD	0–100 kPa	±0.1 % F.S
Mass flow rate	Coriolis mass flow meter	800–8,000 kg/h (water) 0–3,000 kg/h (R123) 300–3,000 kg/h (oil)	±0.2 % flow rate
Rotating speed	JN338 rotational sensor	0–100 N m	0.5 % F.S
Shaft torque	JN338 rotational sensor	0–6,000 r/min	1.0 r/min

Table 3 The main operating parameters in this study

Parameters	Value
Temperature of the conductive oil	150 °C
Mass flow rate of the conductive oil	(2,025 ± 10) kg/h
Temperature of the cooling water	15.4–19.7 °C
Mass flow rate of the cooling water	(2,600 ± 5) kg/h
Shaft torque	10 %–50 % of the maximum value
R123 pumping frequency	5.0–11.0 Hz

3 Results and discussion

3.1 The constant mass flow rate operating mode

Figure 3 shows the shaft torque of the expander. The very stable control of the shaft torque at each level was demonstrated. The expander quickly followed the change of the shaft torque when a new torque value was set. Figure 4 shows the R123 flow rates, which were measured by a Coriolis mass flow meter. The mass flow rate did not change apparently, and the average value was about 680 kg/h at different shaft torque levels. The mass flow rate was generally stable, and its stability was enhanced for the shaft torque larger than 30 % of the maximum value. When

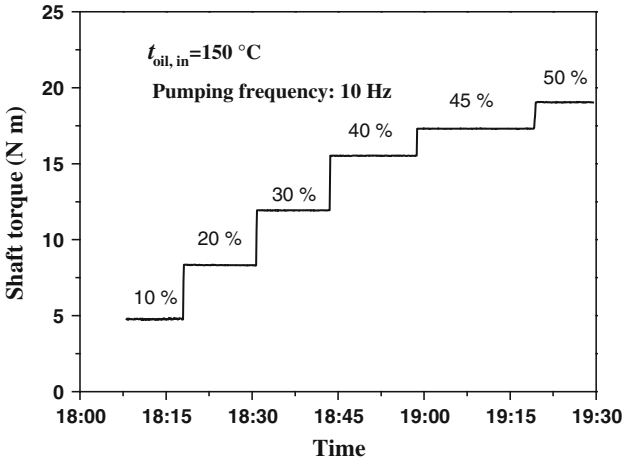

Fig. 3 The step increase of the shaft torque versus time

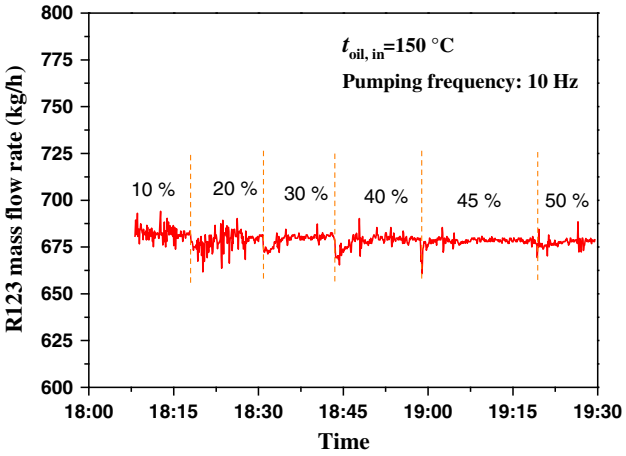

Fig. 4 (Color online) The R123 mass flow rates at different shaft torque levels

the shaft torque suddenly changed, the mass flow rate had a sharp decrease and then was recovered to the stable level in a few minutes. The sharp increase of the shaft torque of the expander directly decreased the expander rotating speed to lower the volume flow rate through the expander. Thus, the R123 fluid pressure in the condenser decreased. This effect decreased the pressure at the pump inlet, leading to a sharp reduction of the R123 flow rate.

Figure 5 shows pressures, temperatures and vapor superheats at the expander inlet. The increase of the shaft torque led to the decrease in the expander rotating speed. As a result, the volume flow rate also decreased. Thus, the vapor pressure at the expander inlet was increased to maintain the constant mass flow rate (see Fig. 5a). The vapor pressure followed the change of the shaft torque in a few minutes, and it was increased by about 80 kPa for each shaft torque increase by 10 %. No apparent pressure overshot and fluctuation were observed. The R123 saturation temperature in the evaporator was increased due to the increase in the pressure. At this condition, the sensible heat of R123 in the evaporator was enlarged, and the latent heat of R123 was reduced. More heat transfer area was occupied by liquid. The combine effect of the heat transfer and fluid flow in the evaporator resulted in the decrease of the heat received from the conductive oil (see Table 4). Consequently, the vapor temperature at the expander inlet decreased (see Fig. 5b). The vapor superheat was defined as the vapor temperature subtracting the saturation temperature, which was an important parameter to influence the ORC system. The previous studies showed that the decreased vapor superheat would increase the thermal efficiency of the ORC system [2, 11]. Because the vapor temperature was decreased and the saturation temperature was increased, the vapor superheat was decreased following the shaft torque rise (see Fig. 5c).

The vapor temperatures had slower response to the shaft torque than the vapor pressures. This effect was more apparent at smaller shaft torques (see Fig. 5b). Later, we will show that the slow transient of the vapor temperatures had much little influence on the ORC performance. Thus, the testing time at each shaft torque level majorly depended on the vapor pressures, not on the vapor temperatures. The vapor temperature was decreased by a couple of degrees at each increment of the shaft torque. It was decreased from 145 to 120 °C in 20 min corresponding to the increase of the shaft torque from 10 % to 50 % of the maximum value.

Figure 6 shows the pressures and temperatures at the expander outlet. The pressures were sharply decreased and then quickly recovered to a stable value following the shaft torque increase. The general trend was the slight decrease of the pressures at the expander outlet with increases in the shaft torques due to the decrease in the heat transfer load in

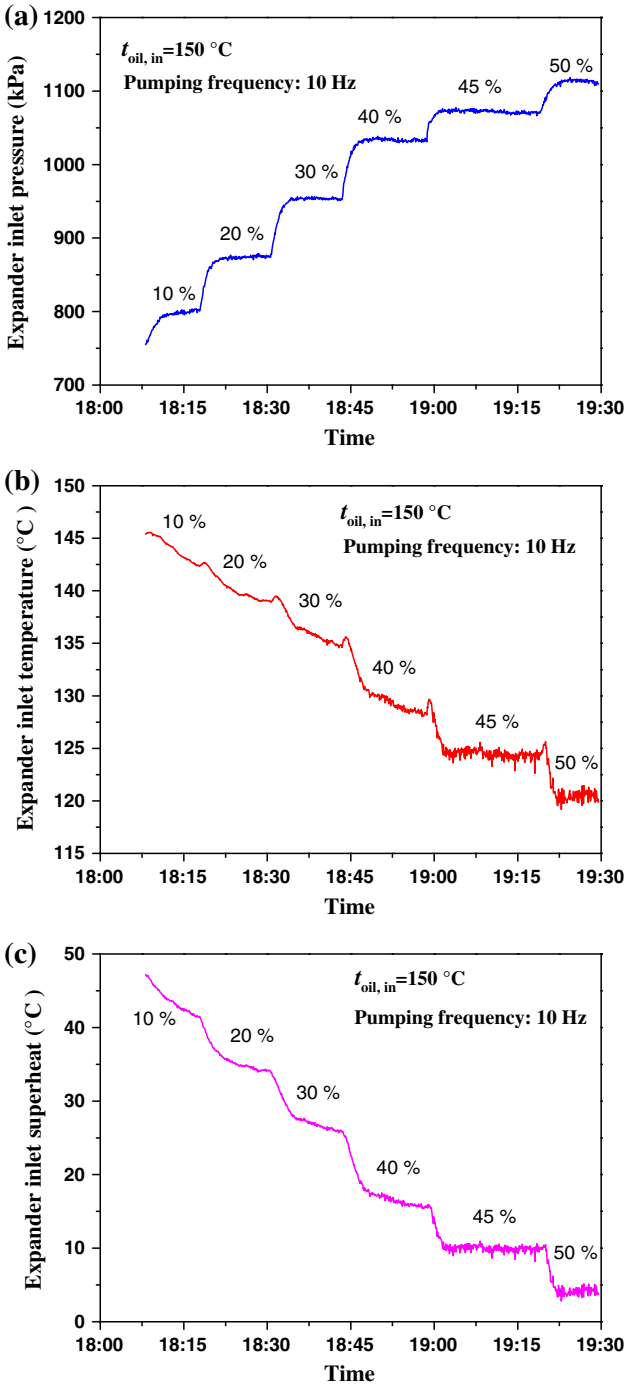

Fig. 5 (Color online) The pressures (**a**), temperatures (**b**) and vapor superheats (**c**) at the expander inlet at different shaft torque level

the condenser. Meanwhile, the temperatures at the expander outlet were decreased by the steep rise of the shaft torque. Figures 5 and 6 indentified the increased expansion ratios in the expander when the shaft torque was raised, due to the increased and decreased pressures at the expander inlet and outlet, respectively.

Figure 7 shows the rotating speed and shaft power of the expander. The rotating speed had a general decrease trend

Table 4 The major ORC performance parameters in this study

m (kg/h)	T (N m)	Q (kW)	$W_{t,me}$ (kW)	R	$\eta_{t,s}$ (%)	$W_{p,me}$ (kW)	η_{me} (%)	$W_{t,cal}$ (kW)	$W_{p,cal}$ (kW)	η_{cal} (%)
682	4.78	48.42	1.402	3.10	53.84	0.69	1.47	2.30	0.33	4.07
680	8.31	47.55	2.046	3.42	61.93	0.72	2.78	2.81	0.35	5.17
680	11.91	46.64	2.430	3.78	65.13	0.74	3.63	3.10	0.38	5.83
679	15.48	45.32	2.593	4.15	65.71	0.77	4.02	3.22	0.35	6.33
678	17.32	43.97	2.615	4.33	65.99	0.77	4.20	3.25	0.39	6.50
678	18.99	43.03	2.538	4.56	64.85	0.75	4.15	3.23	0.37	6.64
330	15.30	23.99	1.650	4.31	87.92	0.38	5.31	2.37	0.10	9.46
400	15.50	29.05	1.955	4.33	82.80	0.45	5.17	2.70	0.16	8.74
473	15.50	34.18	2.239	4.32	78.45	0.53	5.01	2.99	0.21	8.13
544	15.50	39.04	2.497	4.28	74.92	0.60	4.85	3.24	0.27	7.61
611	15.50	42.59	2.600	4.19	70.37	0.68	4.51	3.27	0.20	7.21
680	15.50	45.08	2.630	4.12	67.52	0.75	4.16	3.28	0.35	6.50
749	15.50	46.85	2.390	4.09	76.86	0.85	3.29	3.87	0.43	7.34

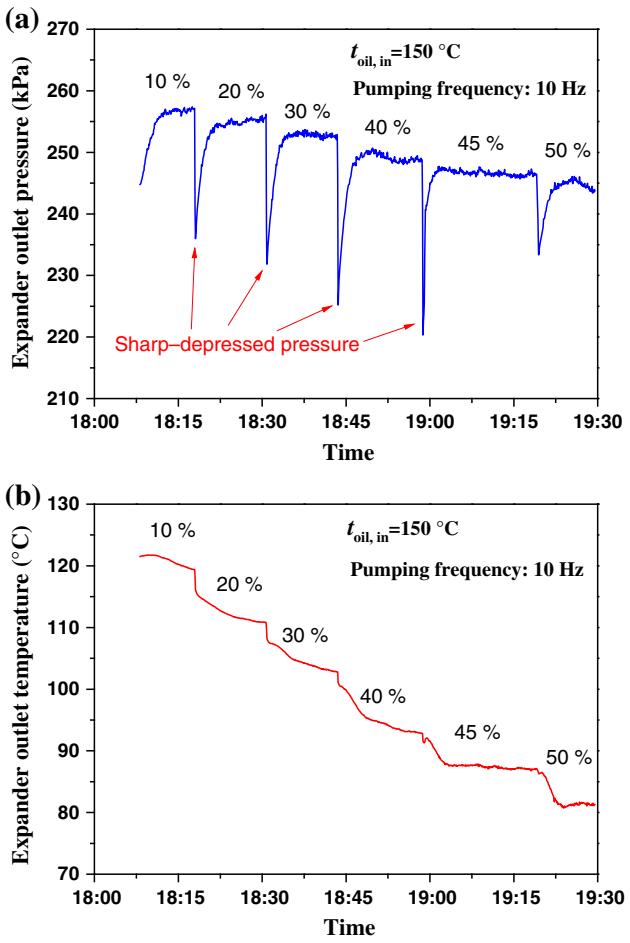

Fig. 6 (Color online) The pressures (**a**) and temperatures (**b**) at the expander outlet at different shaft torque level

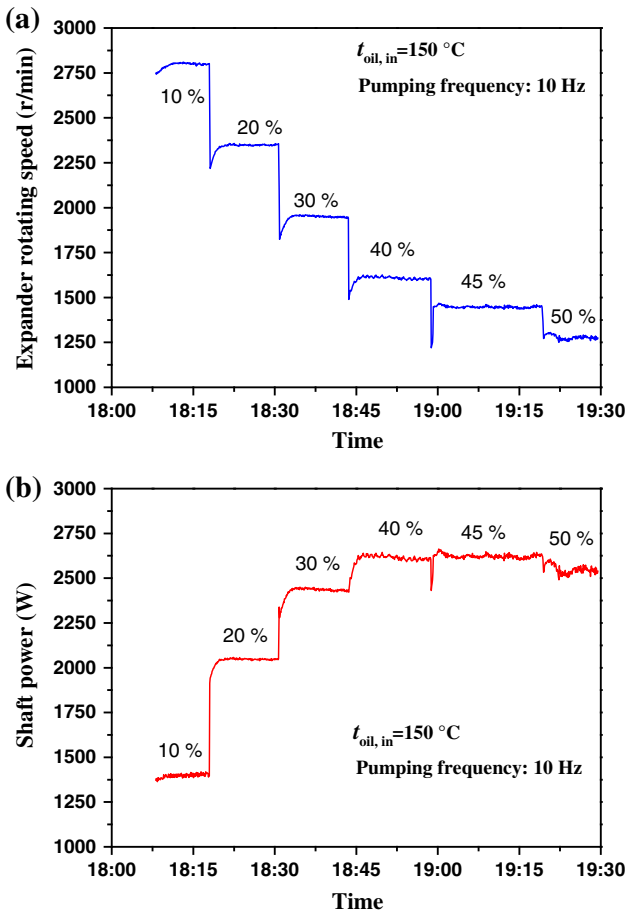

Fig. 7 (Color online) The rotating speed (**a**) and shaft power (**b**) of the expander at different shaft torque level

when the shaft torque was increased. At each shaft torque level, the rotating speed was very stable. However, the sharp-depressed-speed phenomenon was observed just following the sudden increase of the shaft torque. The shaft power could directly provide the mechanical work or generate electricity. It was an important parameter to characterize the ORC performance. Figure 7b shows the increased values of the shaft

power with the increase in the shaft torques. However, the shaft power did not change anymore beyond the 40 % maximum shaft torque. The maximum shaft power was called the saturation shaft power, specifying the limit power that one could use for practical utilizations.

3.2 The constant shaft torque operating mode

This section describes the constant shaft torque operating mode. Here, the shaft torque of the expander was fixed as 15.5 N m. The frequency converter of the piston pump determined the R123 flow rates. The pumping frequency was increased from 5 to 11 Hz by each step of 1 Hz. The 1 Hz frequency corresponded to the flow rate of about 70 kg/h. Figure 8 shows the mass flow rates at each pumping frequency. It can be seen that the mass flow rates could quickly follow the change of the pumping frequency without apparent time delay. The flow rates were oscillating at low pumping frequencies less than 9 Hz due to piston pump performance. The maximum oscillation amplitude was about 15 kg/h even though a damper was installed at the pump outlet to flatten the oscillation. The flow rates were stable without apparent oscillation beyond the pumping frequency of 9 Hz.

Figure 9 shows the vapor pressures, temperatures and superheats at the expander inlet, which exhibits the increased pressures by the step increase of the pumping frequencies (see Fig. 9a). The constant shaft torque operating mode consisted of two regions: the fixed expander temperature (FET) region and the decreased expander temperature (DET) region. The two regions were interfaced at the pumping frequency of 9 Hz (see Fig. 9b). The expander inlet temperatures were relatively constant for the pumping frequencies of less than 9 Hz, but they were sharply reduced beyond the pumping frequency of 9 Hz.

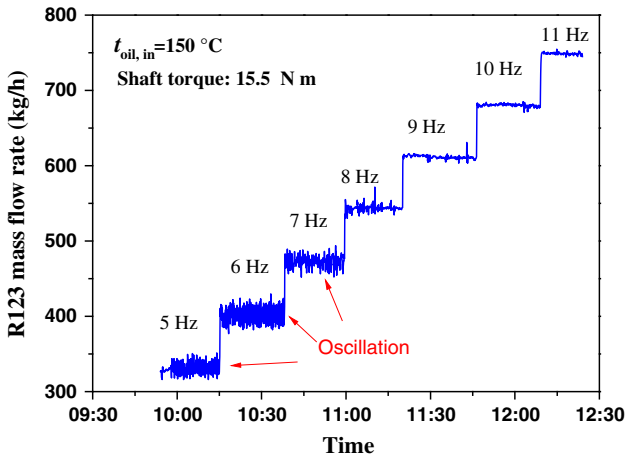

Fig. 8 (Color online) The R123 mass flow rates followed by the change of pumping frequencies

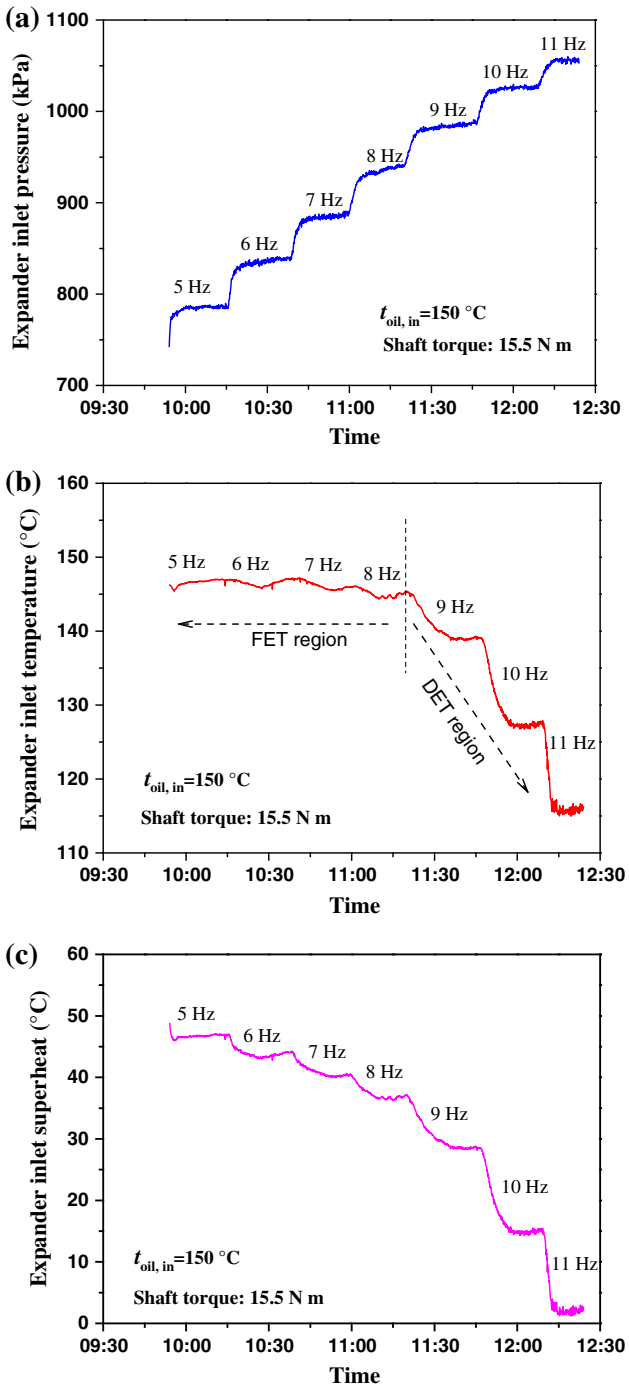

Fig. 9 (Color online) The pressures (**a**), temperatures (**b**) and vapor superheats (**c**) at the expander inlet at each pumping frequency level (FET refers to fixed expander temperature, DET refers to decreased expander temperature)

We note that the whole evaporator length consisted of a subcooled liquid section, an evaporating isothermal section and a superheated vapor section. The operating pressure and R123 mass flow rate influenced the lengths of these sections and the heat received from the heat source. In the FET region, the mass flow rate was relatively small. The

evaporator had sufficient heat transfer area. Thus, the superheated vapor section was significantly long to have a higher vapor temperature at the evaporator outlet, which was only several degrees lower than that of the conductive oil. Thus, the vapor temperature at the expander inlet was maintained to the level of about 146 °C. In the DET region, the increased R123 mass flow rate further shortened the superheated vapor section. Thus, the vapor temperature at the expander inlet was sharply reduced with increases in the R123 flow rates.

There are two factors affecting the vapor superheat at the expander inlet. On the one hand, the increased vapor pressures increased the vapor saturation temperature. On the other hand, the increased R123 flow rates either maintained constant temperatures or decreased temperatures at the expander inlet (see Fig. 9b). Thus, the comprehensive effect caused the decreased vapor superheats at the expander inlet (see Fig. 9c).

Figure 10 shows the pressures and temperatures at the expander outlet. The similar trends of those at the expander inlet can be seen. The expander outlet pressures were increased to a stable value at each new pumping frequency. Because the increased R123 mass flow rate increased the pressure drop in the condenser, the vapor pressure at the expander outlet was raised by about 10–15 kPa at each increase of the pumping frequency. The outlet expander temperatures had similar response as the expander inlet temperatures (see Fig. 9b). They were slightly changed at low pumping frequencies of less than 9 Hz, but were sharply decreased beyond the pumping frequency of 9 Hz. During the whole test, the temperature difference between the expander inlet and outlet was about 40 °C. The expander outlet temperature was about 75 °C at the pumping frequency of 11 Hz, indicating that part of the heat could still be recovered by an internal heat exchanger.

Figure 11 shows the rotating speed and shaft power. We note that the shaft power is the product of the shaft torque and the rotating speed. Because the shaft torque was fixed here, the rotating speed and shaft power are proportional to each other. The two parameters were increased at the pumping frequency of less than 10 Hz, but they attained the saturation values beyond the pumping frequency of 10 Hz.

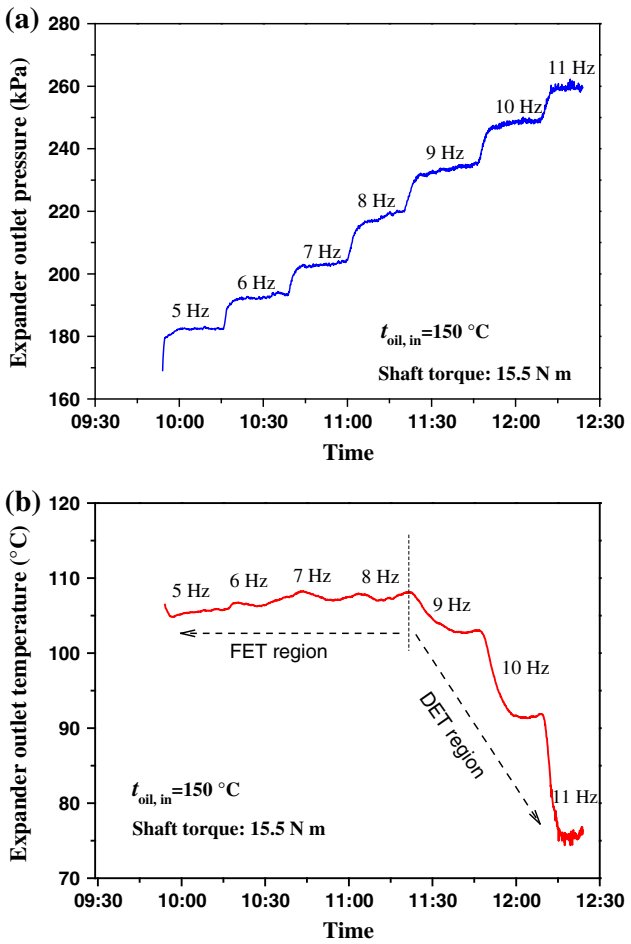

Fig. 10 (Color online) The pressures (**a**) and temperatures (**b**) at the expander outlet at each pumping frequency level

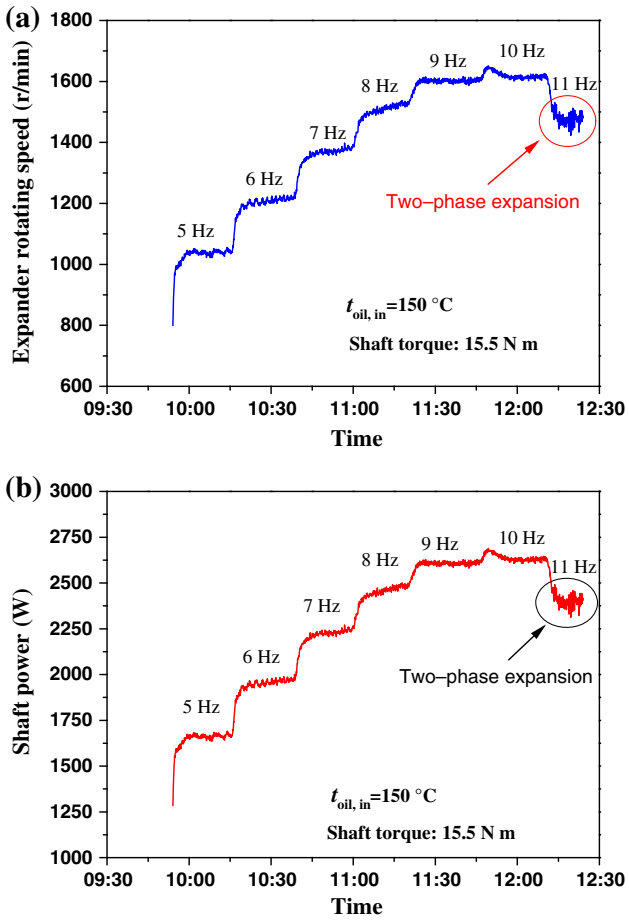

Fig. 11 (Color online) The rotating speed (**a**) and shaft power (**b**) of the expander at each pumping frequency level

The phenomenon of saturation rotating speed and shaft power was explained here. We note that the mass flow rate is the product of the volume flow rate and the vapor density, while the volume flow rate is determined by the expander rotating speed. Thus, the increase of the mass flow rate can be caused by the increases of the rotating speed and/or the vapor density. When the rotating speed attained a specific value, various exergy destructions in the expander limited the further rise of the rotating speed. Under such circumstance, the increased mass flow rates were majorly caused by the increased vapor density in the expander. Thus, the saturation rotating speed and shaft power were reached.

In addition to the above findings, this study observed the weakened expander performance when the near-saturated vapor entered the expander. It can be seen from Fig. 9c that the vapor superheat was only a couple of degrees at the pumping frequency of 11 Hz. The so-called two-phase expansion in the expander reduced and fluctuated the rotating speed of the expander, due to the increased resistance when liquid droplets were involved. The slowed rotating speed further decreased the expander shaft power. Thus, the near-saturated vapor condition at the expander inlet should be avoided for the ORC operating.

3.3 The calculated thermal efficiency and shaft power versus the measured values

Table 4 shows the summarized parameters in this study. For each run, the R123 mass flow rate, shaft torque (represented by "*T*"), heat received from the heat source (conductive oil), shaft power, expansion ratio (represented by "*R*"), isentropic efficiency of the expander, pumping power and thermal efficiency were listed, in which the shaft power, pumping power and thermal efficiency were the measured values and processed by Eqs. (7) and (8). The last three rows of Table 4 were the calculated shaft power, pumping power and thermal efficiency, based on the enthalpy difference across each component (see Eqs. (2)–(6)). The enthalpies were determined by the fluid pressures and temperatures at various locations. The following findings were identified.

3.3.1 The isentropic and thermal efficiency

The expander isentropic efficiencies and the ORC thermal efficiencies were different from case to case. For the constant mass flow rate operating mode, the increase of the shaft torque raised the expander isentropic efficiency and the ORC thermal efficiency. Alternatively, for the constant shaft torque operating mode, the increased mass flow rate decreased the expander isentropic efficiency and the ORC thermal efficiency. The expander isentropic efficiencies were in the range of 53.8 %–87.9 %, and the measured ORC thermal efficiencies (subtracting the pumping power) had the range of 3.29 %–5.31 %.

3.3.2 The measured and calculated thermal efficiencies and shaft powers

The available ORC thermal efficiencies were determined by the enthalpy differences across components in the open literature. The measured thermal efficiencies were seldom reported. Here, we compared the measured shaft power, pumping power and thermal efficiency with the calculated values (see the last three columns in Table 4). The measured shaft power and ORC thermal efficiency were lower than the enthalpy determined values. The measured pumping powers were larger than the enthalpy determined values. The calculated ORC thermal efficiencies were in the range of 4.07 %–9.46 % at the heat source temperature of about 150 °C, which were consistent with the predicted values reported in Refs. [18, 22]. The measured ORC thermal efficiencies were about 53 %–65 % of the calculated values. For instance, the maximum measured thermal efficiency was 5.31 %, which was 56 % of the calculated value (9.46 %). The losses mentioned in Sect. 2.1.2 shrink the power output and cannot be reflected in the measured temperature and pressure.

It is noted that the losses of the shaft power and thermal efficiency were different for different expanders. These data should be further collected for practical ORC applications. Based on this study, the scroll expander could convert about 5.3 % of the heat into useful power at the heat source temperature of 150 °C.

4 Conclusions

Even though there are many studies on ORCs, the development of ORCs is still in the infancy stage. Most of previous studies focused on the thermodynamic analysis of the ORCs. The detailed measurements of various parameters were seldom reported. This study reported the design, construction and test of an ORC with R123 as the working fluid. The scroll expander was modified from a bus-used compressor for air-conditioning systems. The shaft torque, rotating speed and shaft power of the expander were measured by an AC dynamometer unit. The ORC system could be operating well either in the constant mass flow rate operating mode, or in the constant shaft torque operating mode. The detailed response with respect to the changed shaft torque or the mass flow rate was thoroughly analyzed. For both operating modes, it was found that the shaft power could reach a saturation value that was the maximum value one could use. Various exergy destructions in the expander limited the further growth of the shaft

power of the expander. The measured shaft power and ORC thermal efficiency were lower than the enthalpy determined values. At the heat source temperature of 150 °C, the maximum thermal efficiency and shaft power reached about 5.3 % and 2.63 kW, in contrast to the enthalpy determined values of about 9.5 % and 3.87 kW.

Acknowledgments This work was supported by the National Basic Research Program of China (2011CB710703) and the National Natural Science Foundation of China (51306048, 51210011).

References

1. Hung TC, Shai TY, Wang SK (1997) A review of Organic Rankine Cycles (ORCs) for the recovery of low grade waste heat. Energy 22:661–667
2. Chen Q, Xu J, Chen H (2012) A new design method for Organic Rankine Cycles with constraint of inlet and outlet heat carrier fluid temperatures coupling with the heat source. Appl Energy 98:562–573
3. Xu J, Liu C (2013) Effect of the critical temperature of organic fluids on supercritical pressure Organic Rankine Cycles. Energy 63:109–122
4. Andersen WC, Bruno TJ (2005) Rapid screening of fluids for chemical stability in Organic Rankine Cycle applications. Ind Eng Chem Res 44:5560–5566
5. Liu BT, Chien KH, Wang CC (2004) Effect of working fluids on Organic Rankine Cycle for waste heat recovery. Energy 29:1207–1217
6. Saleh B, Koglbauer G, Wendland M et al (2007) Working fluids for low-temperature Organic Rankine Cycles. Energy 32: 1210–1221
7. Tchanche BF, Papadakis G, Lambrinos G et al (2009) Fluid selection for a low-temperature solar Organic Rankine Cycle. Appl Therm Eng 29:2468–2476
8. Tung TC, Wang SK, Kuo CH et al (2010) A study of organic working fluids on system efficiency of an ORC using low-grade energy sources. Energy 35:1403–1411
9. Lai NA, Wendland M, Fischer J (2011) Working fluids for high-temperature Organic Rankine Cycles. Energy 36:199–211
10. Hung TC (2001) Waste heat recovery of Organic Rankine Cycle using dry fluids. Energy Convers Manage 42:539–553
11. Mago PJ, Chamra LM, Somayaji C (2007) Performance analysis of different working fluids for use in Organic Rankine Cycles. Proc Inst Mech Eng Part A- J Power Energy 221:255–264
12. Chen H, Goswami DY, Stefanakos EK (2010) A review of thermodynamic cycles and working fluids for the conversion of low-grade heat. Renew Sustain Energy Rev 14:3059–3067
13. Yamamoto T, Furuhata T, Arai N et al (2001) Design and testing of the Organic Rankine Cycle. Energy 26:239–251
14. Mathias JA, Jon R, Johnston J et al (2009) Experimental testing of gerotor and scroll expander used in, and energetic and exergetic modeling of, an Organic Rankine Cycle. J Energy Resour ASME 131:012201
15. Lemort V, Quoilin S, Cuevas C et al (2009) Testing and modeling a scroll expander integrated into an Organic Rankine Cycle. Appl Therm Eng 29:3094–3102
16. Quoilin S, Lemort V, Lebrun J (2010) Experimental study and modeling of an Organic Rankine Cycle using scroll expander. Appl Energy 87:1260–1268
17. Declaye S, Quoilin S, Guillaume L et al (2013) Experimental study on an open-drive scroll expander integrated into an ORC (Organic Rankine Cycle) system with R245fa as working fluid. Energy 55:173–183
18. Pei G, Li J, Li Y et al (2011) Construction and dynamic test of a small-scale Organic Rankine Cycle. Energy 36:3215–3223
19. Li J, Pei G, Li Y et al (2012) Energetic and exergetic investigation of an Organic Rankine Cycle at different heat source temperatures. Energy 38:85–95
20. Li J, Pei G, Li Y et al (2013) Examination of the expander leaving loss in variable Organic Rankine Cycle operation. Energy Convers Manage 65:66–74
21. Bracco R, Clemente S, Micheli D et al (2013) Experimental tests and modelization of a domestic-scale ORC (Organic Rankine Cycle). Energy 58:107–116
22. Li MQ, Wang JF, He WF et al (2013) Construction and preliminary test of a low-temperature regenerative Organic Rankine Cycle (ORC) using R123. Renew Energy 57:216–222
23. Manolakos D, Papadakis G, Kyritsis S et al (2007) Experimental evaluation of an autonomous low-temperature solar Rankine cycle system for reverse osmosis desalination. Desalination 203:366–374
24. Manolakos D, Kosmadakis G, Kyritsis S et al (2009) Identification of behaviour and evaluation of performance of small scale low-temperature Organic Rankine Cycle system coupled with a RO desalination unit. Energy 34:767–774
25. Manolakos D, Kosmadakis G, Kyritsis S et al (2009) On site experimental evaluation of a low-temperature solar organic Rankine cycle system for RO desalination. Sol Energy 83: 646–656
26. Wang JL, Zhao L, Wang XD (2010) A comparative study of pure and zeotropic mixtures in low-temperature solar Rankine cycle. Appl Energy 87:3366–3373
27. Wang XD, Zhao L, Wang JL et al (2010) Performance evaluation of a low-temperature solar Rankine cycle system utilizing R245fa. Sol Energy 84:353–364
28. Wang XD, Zhao L, Wang JL (2011) Experimental investigation on the low-temperature solar Rankine cycle system using R245fa. Energy Convers Manage 52:946–952
29. Wang JL, Zhao L, Wang XD (2012) An experimental study on the recuperative low temperature solar Rankine cycle using R245fa. Appl Energy 94:34–40
30. Zheng N, Zhao L, Wang XD et al (2013) Experimental verification of a rolling-piston expander that applied for low-temperature Organic Rankine Cycle. Appl Energy 112:1265–1274